Maaskant *et al. Animal Microbiome* (2025) 7:39
https://doi.org/10.1186/s42523-025-00410-2

Animal Microbiome

RESEARCH Open Access

AI for rapid identification of major butyrate-producing bacteria in rhesus macaques (*Macaca mulatta*)

Annemiek Maaskant[1,2*†], Donghyeok Lee[3†], Huy Ngo[3], Roy C. Montijn[3], Jaco Bakker[1], Jan A. M. Langermans[1,2] and Evgeni Levin[3*]

Abstract

Background The gut microbiome plays a crucial role in health and disease, influencing digestion, metabolism, and immune function. Traditional microbiome analysis methods are often expensive, time-consuming, and require specialized expertise, limiting their practical application in clinical settings. Evolving artificial intelligence (AI) technologies present opportunities for developing alternative methods. However, the lack of transparency in these technologies limits the ability of clinicians to incorporate AI-driven diagnostic tools into their healthcare systems. The aim of this study was to investigate an AI approach that rapidly predicts different bacterial genera and bacterial groups, specifically butyrate producers, from digital images of fecal smears of rhesus macaques (*Macaca mulatta*). In addition, to improve transparency, we employed explainability analysis to uncover the image features influencing the model's predictions.

Results By integrating fecal image data with corresponding metagenomic sequencing information, the deep learning (DL) and machine learning (ML) algorithms successfully predicted 16 individual bacterial genera (area under the curve (AUC) > 0.7) among the 50 most abundant genera in rhesus macaques (*Macaca mulatta*). The model was successful in predicting functional groups, major butyrate producers (AUC 0.75) and a mixed group including fermenters and short-chain fatty acid (SCFA) producers (AUC 0.81). For both models of butyrate producers and mixed fermenters, the explainability experiments revealed no decline in the AUC when random noise was added to the images. Increased blurring led to a gradual decline in the AUC. The model's performance was robust against the impact of fecal shape from smearing, with a stable AUC maintained until patch 4 for all groups, as assessed through scrambling. No significant correlation was detected between the prediction probabilities and the total fecal weight used in the smear; $r = 0.30 \pm 0.3$ ($p > 0.1$) and $r = 0.04 \pm 0.36$ ($p > 0.8$) for the butyrate producers and mixed fermenters, respectively.

†Annemiek Maaskant and Donghyeok Lee contributed equally to this work and are first authors.

*Correspondence:
Annemiek Maaskant
maaskant@bprc.nl
Evgeni Levin
evgeni.levin@horaizon.nl

Full list of author information is available at the end of the article

Conclusion Our approach demonstrated the ability to predict a wide range of clinically relevant microbial genera and microbial groups in the gut microbiome based on digital images from a fecal smear. The models proved to be robust to the smearing method, random noise and the amount of fecal matter. This study introduces a rapid, non-invasive, and cost-effective method for microbiome profiling, with potential applications in veterinary diagnostics.

Keywords Microbiome, SCFA, Monkeys, Gut health, Artificial intelligence, Diet, Diarrhea, Butyrate producer, Explainability analysis

Background

The gut microbiome plays a pivotal role in shaping mammalian health and susceptibility to disease [1, 2]. It influences a wide range of physiological processes, including digestion, nutrient absorption, metabolism, immune function, and even behavior [3–5]. Disruptions in microbiome composition and function, known as dysbiosis, have been linked to various diseases, such as inflammatory bowel disease [4, 6–8].

Dysbiosis has been implicated in the development of diarrhea in nonhuman primates (NHPs) [9]. In captive NHPs, such as rhesus macaques (*Macaca mulatta*), diarrhea is a common health and welfare concern [10–12]. A better understanding of their microbiome functions will improve healthcare interventions and welfare in these captive populations [1, 2, 9, 13]. Although gut microbiome analysis is a commonly used method in NHPs, these techniques are expensive, time-consuming, and require specialized laboratory facilities and bioinformatics expertise. This limits its accessibility for routine clinical use, especially in veterinary practice [9, 13–17]. The clinical interpretability of this intricate microbiome dataset can be improved by identifying functional groups, such as bacterial populations that ferment dietary fibers and thereby produce butyrate. Butyrate, a key short-chain fatty acid (SCFA), is essential for maintaining intestinal health. It serves as a primary energy source for colonocytes, reduces inflammation, and supports gut barrier integrity, contributing to overall gut health [18, 19].

Microbiome research has been revolutionized with the use of artificial intelligence (AI). Subsets of AI, such as machine learning (ML) and deep learning (DL), have proven to be efficient in analyzing complex and large datasets [20]. ML and DL can offer selection, biomarker identification, disease prediction, and treatment recommendations, providing insights into microbiome structure and dynamics [21, 22]. Thus, ML has been used to explore the predictive power of the microbiota in relation to animal phenotypes in ruminants and dogs [23–25]. In addition, DL has been used to identify eukaryotic sequences in biomass from the rumen [9]. These methods rely on the metagenomic sequencing data of the targeted microbiome. The ability to profile the intestinal microbiome by using only an image of a fecal smear would allow a predictive, preventative, and personalized approach for health monitoring. Recent studies have demonstrated that AI models can analyze images of fecal samples to assess microbiome composition [26–29]. By leveraging algorithms, these models can capture subtle visual cues linked to microbial communities, providing clinically relevant insights into gut health without extensive laboratory work.

Beyond its efficiency, explainability in AI is crucial in healthcare because it enhances trust by making the AI decision-making process transparent. This transparency allows healthcare professionals to clearly understand how AI-derived outcomes are formulated, ensuring the reliability and scientific validity of these technologies [30]. Furthermore, identifying the features driving the model's predictions increases confidence in its outputs so that the results are biologically meaningful.

Here, we present an advanced ML- and DL-based method for the rapid identification of key bacterial genera and functional groups, specifically major butyrate producers, from digital images of fecal smears of rhesus macaques. By integrating fecal imaging with learning algorithms that have been trained on corresponding metagenomic sequencing data, our approach can predict key microbial genera and functional groups with high accuracy. To explore the interpretability and trustworthiness of our model, we employed explainability analysis to uncover the image features influencing the model's predictions with respect to the smearing method, sample weight, and random noise. Profiling the microbiome with this ML- and DL-based method has the potential to significantly reduce the cost of assessing the impact of drugs or nutritional interventions on the microbiome.

Methods

Animal subjects, housing, and care

This study utilized fecal samples from a cohort of 14 rhesus macaques *(Macaca mulatta)* involved in a broader research project on gastrointestinal health and nutrition at the Biomedical Primate Research Centre (BPRC, Rijswijk, The Netherlands), as described in detail in Maaskant et al., 2024 [13]. The macaques were fed a diet of commercial monkey pellets supplemented with fresh fruits, vegetables, and grains.

Comprehensive electronic health records were maintained for each animal throughout the study.

Fecal sample collection

The fecal samples were serially collected from 2020 to 2022, adhering to a standardized collection protocol. Food colorants and glitters were used as dietary markers to distinguish individual fecal samples from socially housed macaques. All animals received dietary markers in alternating sequences to exclude a possible influence from these identification methods. The dietary markers were fed to the animals in the afternoon, and the next morning, fecal samples were collected between 9:00 AM and 11:00 AM to minimize variability. Each sample was divided into three aliquots of approximately 1 gram each. For microbiome sequencing, aliquots were immediately frozen at -80 °C. The remainder of the fecal samples were intended for imaging and were stored at -20 °C until analysis.

DNA extraction and metagenomic sequencing

Total genomic DNA was extracted from the fecal samples using a modified protocol designed for high throughput and purity. Briefly, 150 µL of each sample was combined with 500 µL of 0.1 mm zirconium beads and 800 µL of lysis buffer (CD1 solution from the DNeasy 96 PowerSoil Pro QIAcube HT Kit). Mechanical lysis was performed through bead beating for two cycles of 2 min each, with cooling on ice between cycles. Following centrifugation to remove debris, the supernatant was mixed with binding buffer and magnetic beads to facilitate DNA capture. The DNA was then purified using the PurePrep 96 system (Molgen, The Netherlands), which included two wash steps and elution in 65 µL of elution buffer.

For library preparation, the Illumina DNA Prep Kit was used according to the manufacturer's protocol. DNA concentrations were normalized across all samples to ensure uniform library input. The tagmentation step was followed by PCR amplification using indexed adapters, allowing for sample multiplexing. Libraries were purified and pooled, and sequencing was performed on an Illumina MiSeq platform using MiSeq V3 chemistry, generating 2 × 300 bp paired-end reads.

Metagenomic data processing and taxonomic profiling

The raw sequencing reads were subjected to quality control using the fastp tool, which filters out low-quality reads, trims adapter sequences, and removes reads that are too short [31]. High-quality reads were then processed using Kraken2, which employs a custom-built database that includes sequences from Archaea, Bacteria, Plasmids, Viruses, Fungi, and UniVec Core sequences to ensure comprehensive taxonomic assignment [32]. Potential contamination from human DNA was mitigated by including the GRCh38 human genome assembly in the database [33]. Taxonomic classifications were refined using Bracken, which provides more accurate abundance estimates by re-estimating the assignments based on k-mer distributions [34]. All bioinformatics tools were managed through the Bioconda package manager to ensure reproducibility [35].

Fecal imaging procedure

A standardized imaging protocol was used to ensure consistency [28]. Briefly, the fecal samples were smeared onto a custom-designed paper template featuring a central square and fiducial markers at the corners (Fig. 1A). The thawed samples were evenly spread within the central square using a disposable spatula, ensuring uniform coverage (Fig. 1B). Images of the smeared samples were captured using an iPad camera (8-megapixel camera, 9th generation, model MK2K3NF/A, Apple Inc., Cupertino, CA, USA) (Fig. 1C). These images were subsequently uploaded into the model for analysis.

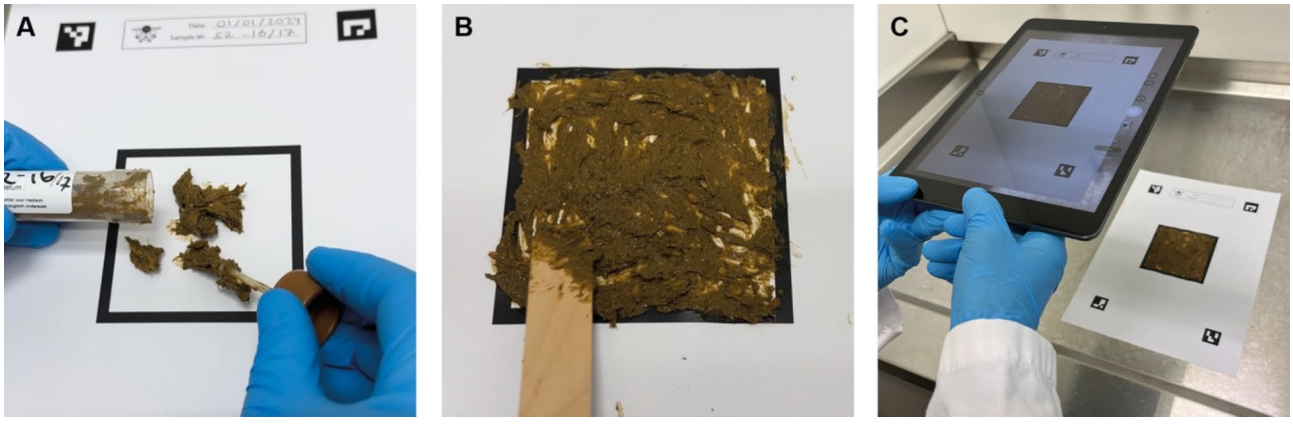

Fig. 1 Adapted from Lee et al. [36]. (**A**) Paper template with feces applied within the borders of the square. (**B**) The fecal layer was smeared as evenly as possible using a disposable spatula. (**C**) Photograph of the smear including the fiducial marks

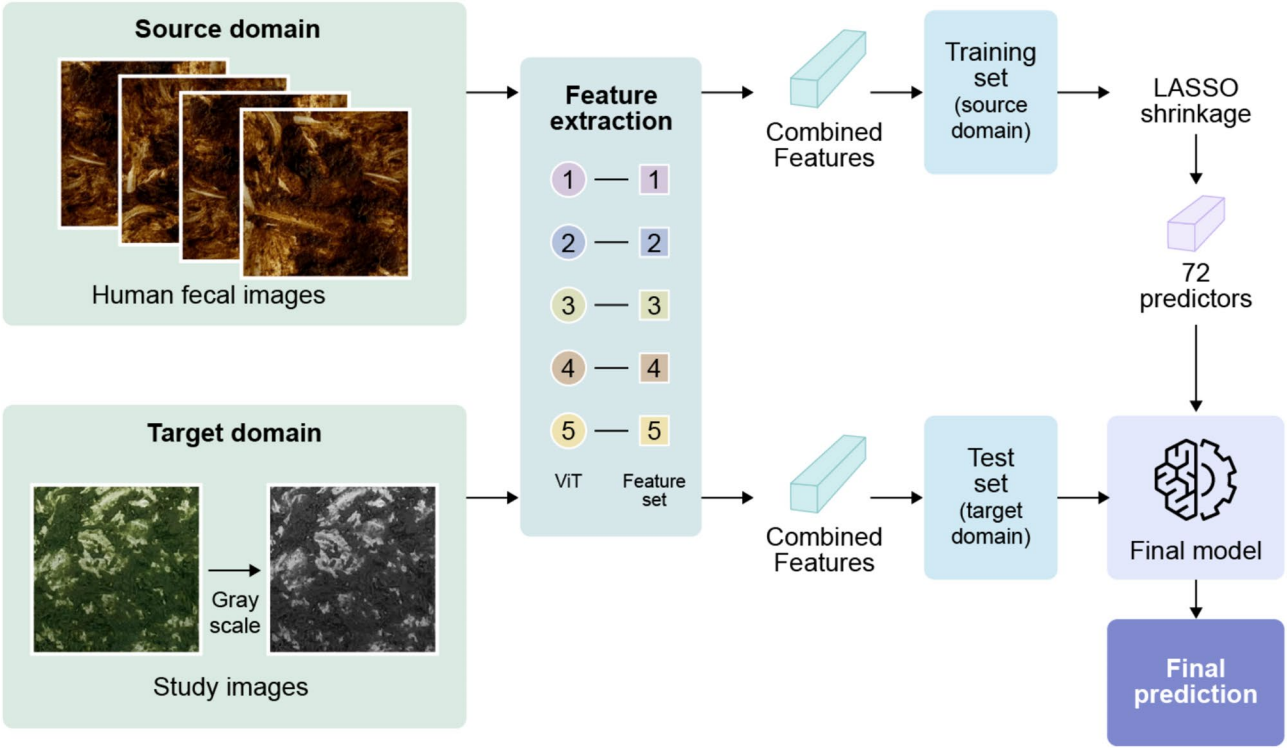

Fig. 2 Pipeline of preprocessing, model training, and evaluation. During preprocessing, the study images were converted to grayscale; the images were then transformed into features. The features were extracted using five different pretrained Vision Transformer (ViT) models. Subsequently, least absolute shrinkage and selection operator (LASSO) regression with additional variance filtering for feature selection were applied, resulting in a reduction to a final feature set of 72 predictors

Table 1 Pretrained vision transformer (ViT) models used for feature extraction

Model	Dataset	Use case
vit_tiny_patch16_224 [37]	ImageNet dataset	Lightweight vision tasks with faster inference, typically applied to ImageNet-like datasets.
vit_large_patch16_224. augreg_in21k_ft_in1k [37, 38]	ImageNet dataset	A larger ViT model for general vision tasks, also trained on ImageNet.
vit_base_patch16_clip_224 [39]	OpenAI's CLIP dataset	Utilizes CLIP's dataset for vision tasks, focusing on robustness to out-of-distribution data.
vit_base_patch16_224_dino [40]	ImageNet dataset	A self-supervised learning model, ideal for unsupervised applications beyond ImageNet-tasks
resnetv2_50×1_bit_distilled [41, 42]	JFT-300 M dataset	Optimized for transfer learning with large-scale datasets like JFT-300 M

Model analysis

A total of 123 fecal smear images were included in this study. To mitigate the potential confounding effects of color variations introduced by dietary markers, all the images were converted to grayscale. This preprocessing step ensured that color differences did not influence the model's predictions, allowing the model to focus on textural and structural features of the fecal smears.

Feature extraction and model training

For training the model, the data from another study were used [29]. To amplify the contrast between high- and low-abundance samples, the images representing the top and bottom 20% of alpha diversity (Shannon index) were selected, resulting in a total of 204 training images. The pipelines used (Fig. 2) consisted of both ML- and DL-based sections. We utilized a DL-based feature extraction approach based on multiple pretrained image classification models. Features were extracted from the grayscale images using a pipeline employing five different pretrained Vision Transformer (ViT) models (Table 1), resulting in approximately 4,800 features per image. The features of each pretrained model represent the comprehensive information in the image data and are integrated into a classifier with ML methods.

The training dataset, consisting of 204 samples with 4800 features each, is a high-dimensional, low-sample-size (HDLSS) scenario with a high risk of overfitting. To

prevent overfitting, we applied least absolute shrinkage and selection operator (LASSO) regression with additional variance filtering for feature selection [43]. This resulted in a reduction to a final feature set of 72 informative predictors. LASSO regression offers built-in feature selection by shrinking noninformative feature coefficients to zero, thus simplifying the model. Although Random Forest achieved a comparable predictive performance of the area under the curve (AUC ~ 0.77), its calibration properties were inferior to those of LASSO. This is demonstrated by a higher expected calibration error (ECE) and a narrower range of predicted probabilities (Fig. 3). In addition, DL models require larger datasets to generalize effectively, which is not feasible for our dataset.

We employed a stratified cross-validation approach during model training on the source domain. The final model was then frozen and applied to the target/test domain. The classifier's performance was evaluated using the area under the curve (AUC) operating characteristic curve, with stratified shuffling split cross-validation (20 shuffles) ensuring robust assessment, with 30% of the data used as the test set [44]. Permutation testing (300 permutations) was conducted to determine whether the observed performance was significantly better than random chance. P values of < 0.05 were considered statistically significant. Analysis and visualization were performed using Python, PyTorch and Scikit-learn [45, 46]. AUC values greater than 0.8 were considered excellent, values between 0.7 and 0.8 were considered very good, values between 0.65 and 0.7 were considered good, values between 0.6 and 0.65 were considered moderate, and values less than 0.6 were considered poor for prediction.

The hyperparameters, including the variance threshold and regularization strength, were optimized using grid search within an inner stratified cross-validation loop. The hyperparameter set for LASSO (λ) and variance filtering (γ) are as follows: the λ values are [0.1, 0.2, 0.3, 0.4, 0.5, 0.6, 0.7, 0.8, 0.9, 1, 10, 100] for the inverse regularization strength of the classifier, and the γ values are set at [0.001, 0.01, 0.05, 1, 2, 2.5] for the variance threshold filter. After the model's performance was evaluated, the final model was retrained on the entire dataset to produce the final predictive model. This model was subsequently used to evaluate the predictive performance for each bacterial genus in the study.

Genera Selection and Labeling.

To focus on bacterial genera that are both prevalent and abundant, we applied a two-step selection process. First, with sparsity filtering, the genera with more than 50% sparsity, i.e., present in less than 50% of the samples, were filtered out. Second, of the remaining genera, the top 50 most abundant genera were selected on the basis of their average relative abundance.

For each selected bacterial genus, we defined binary labels to facilitate the classification task. Specifically, samples in the top 10% of abundance for a given genus were labeled "high," and those in the bottom 10% were labeled "low". This approach resulted in a total of 24 images out of 123 being used for high-low model prediction for each genus. The rationale behind this binary approach is based on model design and statistical power. For model design, most pretrained models are designed for classification tasks rather than regression. For statistical power, focusing on the extremes of the data distribution (top and

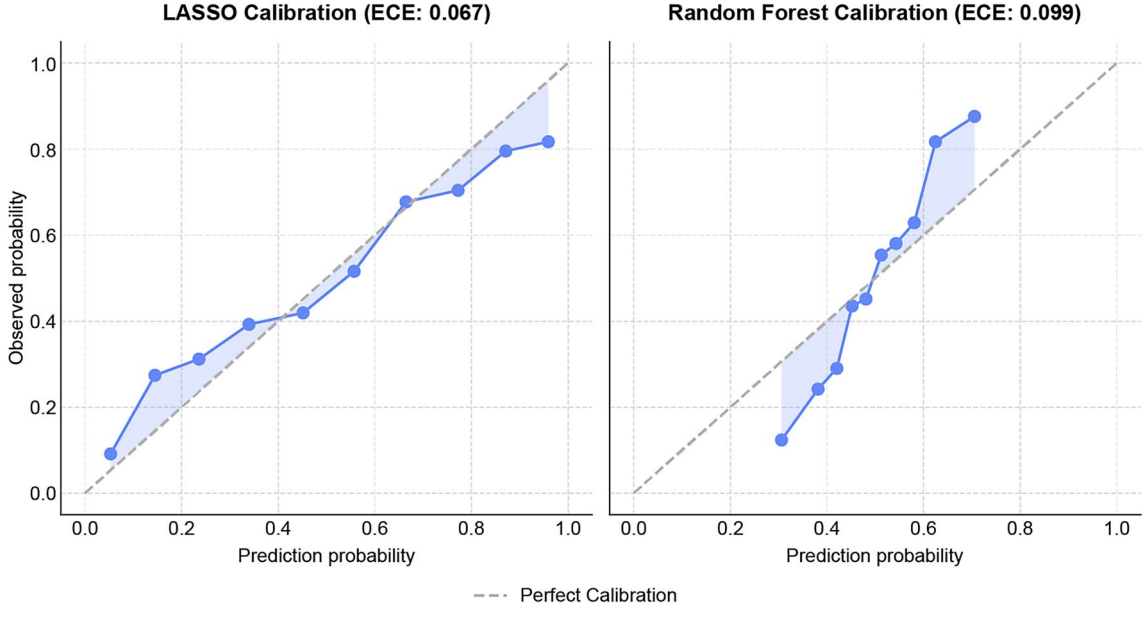

Fig. 3 Calibration curves of least absolute shrinkage and selection operator (LASSO) and random forest, including expected calibration error (ECE), demonstrating a higher ECE and a narrower range of predicted probabilities for random forest than for LASSO

bottom 10%) enhances the effect size, making it feasible to detect significant differences given the limited sample size.

Prediction of functional groups

We extended our analysis to predict functional groups of bacteria, specifically major butyrate producers, and a mixed group including fermenters, other SCFA producers and minor butyrate producers. The twenty-five successful predictive genera (AUC > 0.6) were subsequently assigned to the (A) butyrate producer group or (B) mixed fermenter group. The assignment of genera was based on the main functions described in the literature [18, 47–69]. Both groups were defined based on the sum of the relative abundances of their constituent genera. The group prediction tasks were subjected to the same preprocessing, model training, and evaluation processes as genus prediction.

Model interpretation and robustness analysis

We investigated whether the model performance was influenced by external factors such as the smearing method, random noise, and the amount of feces. Figure 4 illustrates how the smear affects the general shape of the feces on the paper, i.e., the global shape.

To assess the robustness and decision-making of the model, we conducted random noise intervention experiments using blurring, Gaussian noise and scrambling of the images. Figure 5 illustrates how each intervention modifies the original image. Blurring applies a smoothing effect to the images, reducing fine details by averaging pixel values in a local region, and its intensity also increases globally. This experiment evaluates the importance of local information and image quality. Gaussian noise introduces random variations to the images without directly altering image features. This is employed to evaluate the model's robustness to random noise. Scrambling rearranges small patches of the images, disrupting the global shape. This approach assesses the effect of the overall shape created by smearing. At a scrambling size of 2 × 2, the image appears unchanged, and larger scrambling levels destroy both local and global features (Fig. 6).

Results

The pretrained model trained on 204 fecal images achieved an AUC of 0.77 ± 0.05 (Fig. 7). The permutation test yielded a p value less than 0.05, indicating that the model's performance was statistically significant.

Figure 8 shows the AUC of the 50 selected genera based on their relative abundance. The genera that were predicted the best by our model (AUC > 0.8) included *Coprococcus*, *Intestinimonas*, *Dysosmobacter*, *Faecalibacillus*, *Ruminococcus* and *Flavonifractor.*

The 25 genera assigned to the butyrate-producing genera were as follows: *Coprococcus*, *Intestinimonas*, *Dysosmobacter*, *Ruminococcus*, *Flavonifractor*, *Clostridium*, *Flintibacter*, *Catenibacterium*, *Butyrivibrio*, *Eubacterium* and *Enterocloster.* The mixed fermenter group included the following genera: *Faecalibacillus*, *Vescimonas Treponema*, *Ruthenibacterium*, *Phascolarctobacterium*, *Oscillibacter*, *Pusillibacter*, *Pseudomonas*, *Bacillus*, *Streptomyces*, *Clostridioides*, *Sarcina*, *Candidatus*, *Wujia* and *Bacteroides.* For predicting the butyrate producer and mixed fermenter groups, the model achieved AUCs of 0.75 and 0.81, respectively. Permutation tests of both analyses revealed p values < 0.05 (Fig. 9).

Figure 10 summarizes the results of the intervention experiments. In both the mixed fermenter and butyrate producer groups, the blurring intervention resulted in a gradual decline in the AUC as the blurring radius increased. However, for both groups, the model's performance remains unchanged regardless of the noise size, indicating that the model is robust to noise. For the scrambling intervention, the performance remained stable up to 4 patches for the fermenter group and 2 patches for the butyrate group. With a small patch size, this intervention alters the global shape, indicating that the shape created by smearing is insignificant. However, as the patch size increases, it starts to destroy both local and global features, resulting in a substantial decrease in the AUC for 8 patches in the fermenter group and 6 patches in the butyrate group.

Overall, the median amount of feces that was used in the smears was 1.9 g (range 0.36–5.4 g). In both the fermenter and butyrate producer groups, no correlation was

Fig. 4 Smear direction affects the global shape of the smear image

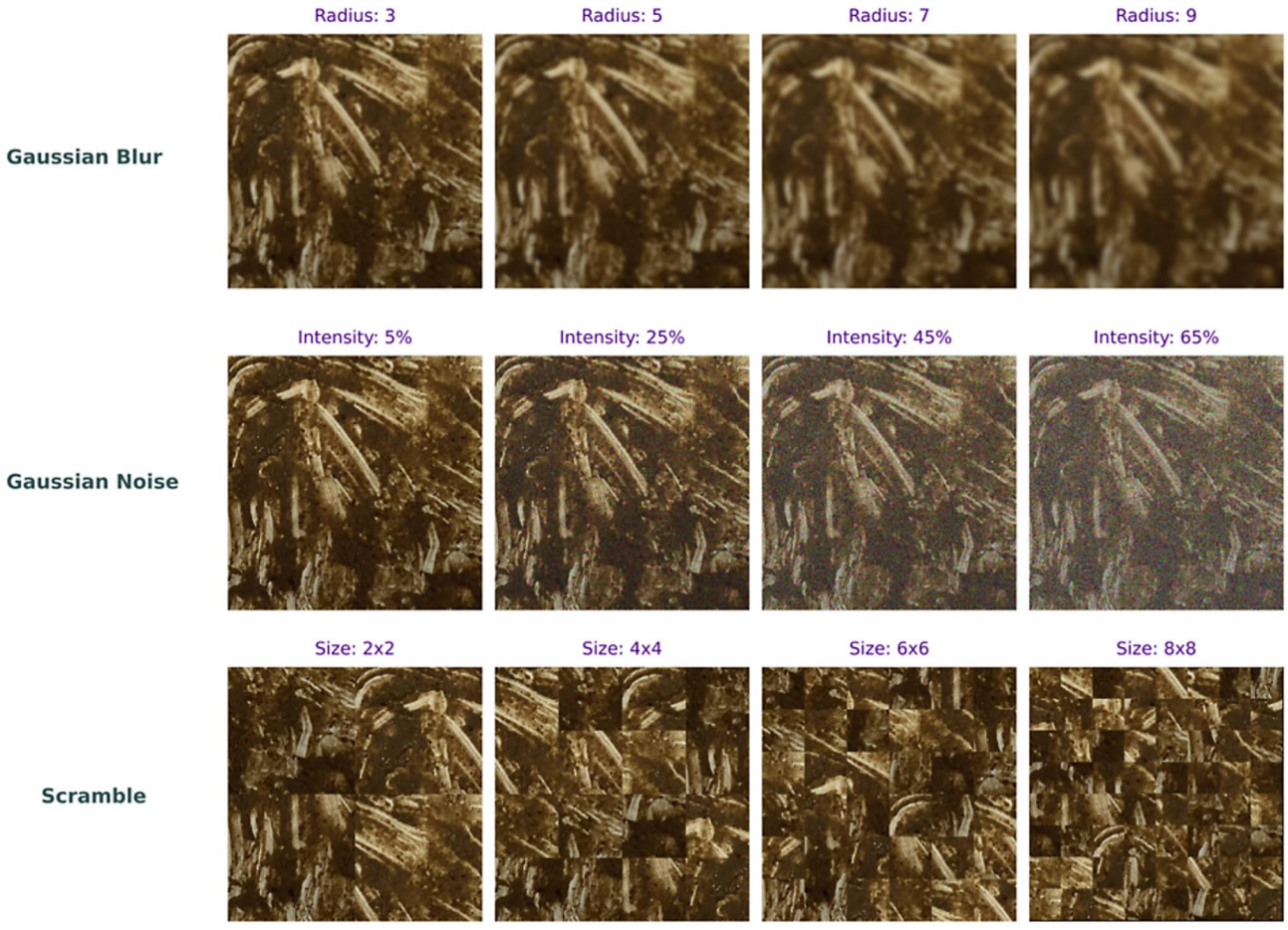

Fig. 5 Overview of interventions on the original image, including Gaussian blur, Gaussian noise, and scrambling at different intervention levels. For illustrative purposes, original colors are used. For the experiment, only grayscale images were used

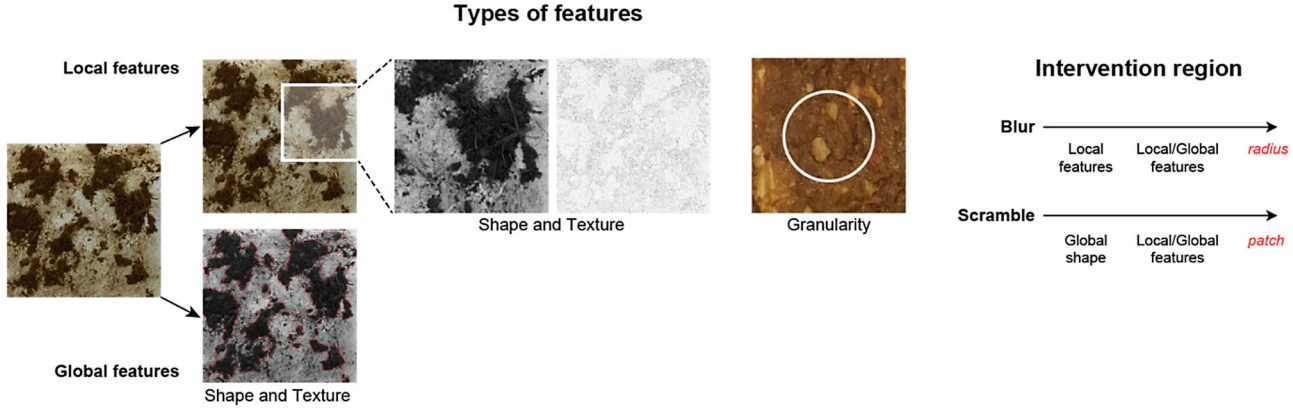

Fig. 6 Properties of image features and the effects of each intervention on local and global features: the blur diminishes local features by averaging pixel values within a radius. At smaller radii, it primarily affects local features, but as the radius increases, it starts to disrupt both local and global features. Scrambling at a small patch level disrupts only the global shape; however, as the patch size increases, it destroys both local and global features

detected between the weight of the fecal smear and the prediction probabilities (Fig. 11). The Pearson correlation coefficients (r) are 0.30 ± 0.3 ($p > 0.1$) and 0.04 ± 0.36 ($p > 0.5$) for the butyrate producers and the mixed fermenter groups, respectively.

Discussion

This study introduces an advanced ML and DL approach (hereafter referred to as the ML/DL model) for the successful prediction of 'high-low' bacterial genera and functional groups in the microbiome from digital images of

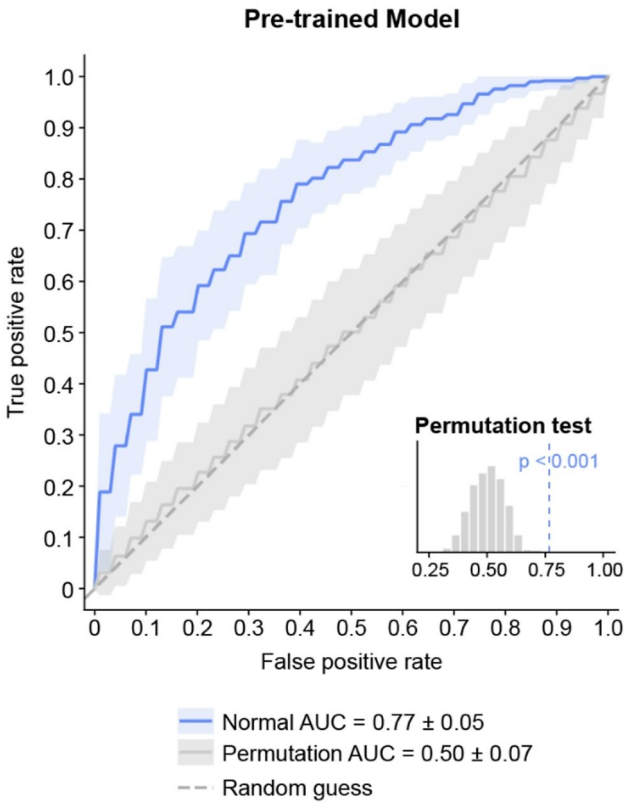

Fig. 7 The area under the receiver operating characteristic curve (AUC), presented as the mean ± SD, with a permutation test and its p value

fecal smears from rhesus macaques. Major butyrate producers and a group of mixed fermenters could be predicted. Additionally, our ML/DL model demonstrated promising predictive capabilities for several bacterial genera, highlighting its potential utility in microbiome analysis and veterinary diagnostics. Our data showed that the model was robust to the smearing method, random noise and amount of fecal matter used for the smear. These results will accelerate the path toward routine clinical application of microbiome analysis using digital images.

In addition to individual genera, the model effectively predicted the presence of major butyrate producers, such as *Coprococcus*, *Ruminococcus*, *Clostridium*, *Butyrivibrio* and *Eubacterium*. The ability to predict butyrate-producing bacteria is clinically valuable, as these microbes play essential roles in maintaining colonic health, modulating immune responses, and protecting against gastrointestinal disorders [18, 59]. A reduced abundance of butyrate producers has been associated with gastrointestinal disorders and chronic diseases such as Long-Covid [70, 71].

The model achieved high predictive accuracy for several important bacterial genera within the major butyrate-producing group, with AUC values exceeding 0.80 for *Coprococcus*, *Dysosmobacter*, *Intestinimonas*, *Ruminococcus*, and *Flavonifractor*. The model's ability to predict butyrate producers as a group and as distinctive genera emphasizes its potential in assessing gut microbial functions related to butyrate production. Moreover, the model also demonstrated good predictive performance, with an AUC > 0.7, for genera in the mixed fermenter group, such as *Faecalibacillus*, *Vescimonas*, *Treponema*, *Ruthenibacterium and Phascolarctobacterium.*

Our results expand upon our previous work, where a limited number of genera were predicted from fecal images [28]. Our current study maximized the dataset size from 66 to 123 images by including images colored by the food-colorant marker [28]. In addition, by using an extensive human training dataset and employing multiple pretrained models, we demonstrated the ability to

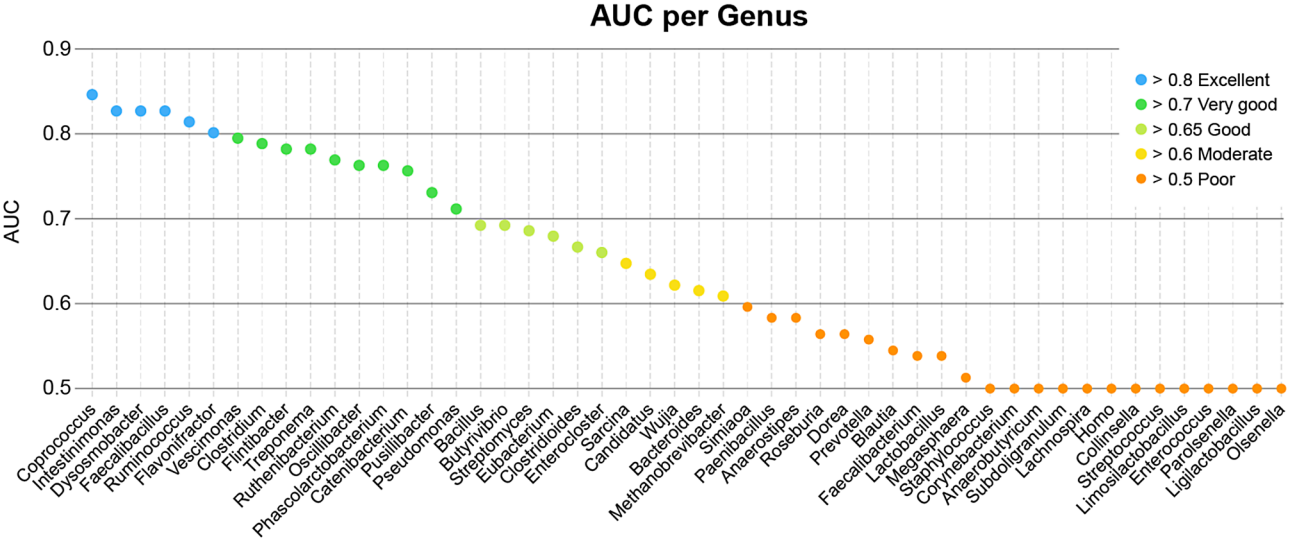

Fig. 8 Results of the area under the receiver operating characteristic curve (AUC) per predicted genus of the 50 most abundant genera. AUC values > 0.8 were considered excellent; 0.7–0.8, very good; 0.65–0.7, good; 0.6–0.65, moderate; and < 0.6, poor for prediction

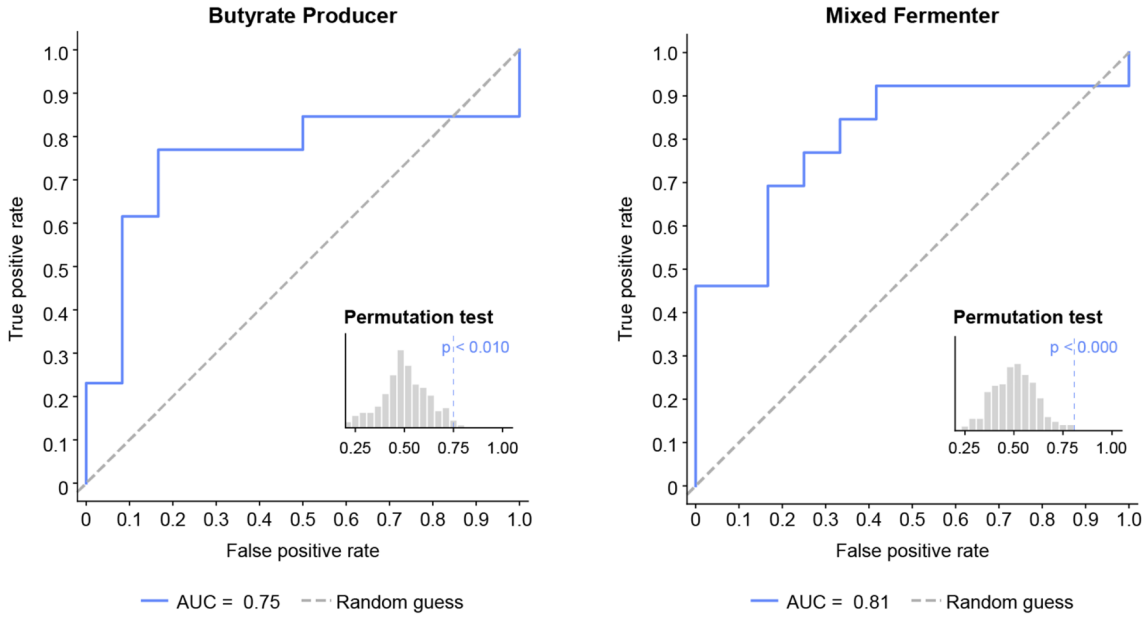

Fig. 9 The area under the receiver operating characteristic curve with a permutation test and its p value for the butyrate producer group (left) and the fermenter group (right)

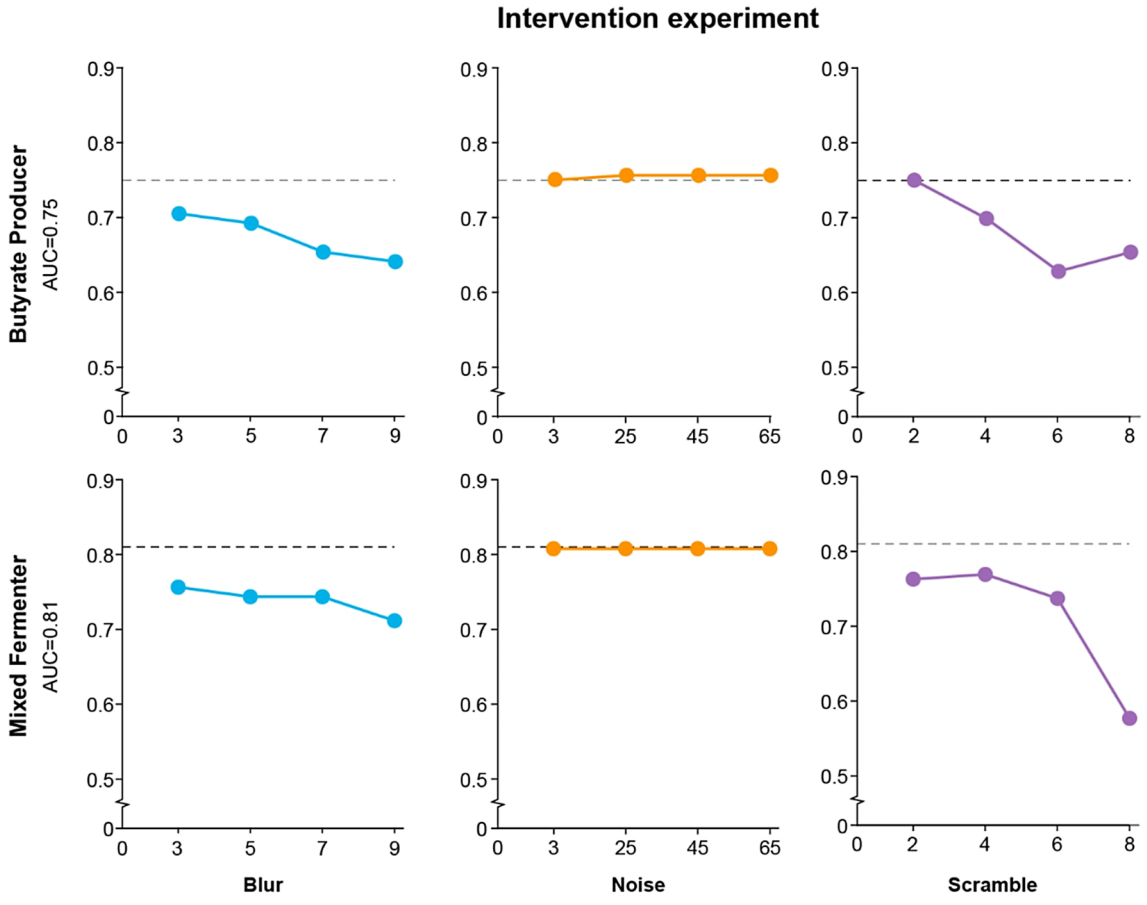

Fig. 10 The area under the curve (AUC) for different intervention methods and their levels. The difference between the baseline, i.e., the performance without intervention, and each AUC reflects the model's robustness and the importance of certain image features

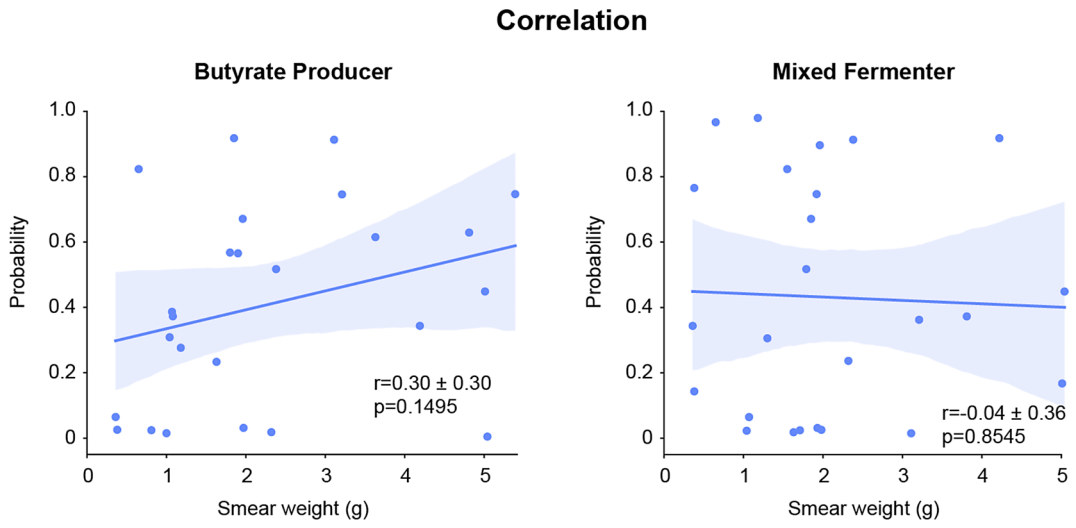

Fig. 11 Correlations between the prediction probabilities and the total fecal weight used in the smear (in grams); **r** indicates the Pearson correlation coefficient (mean± sd), and **p** denotes the p value

predict a broader range of bacterial genera and functional groups [29]. We used the human-derived dataset because of the similarity of many common genera that are shared between humans and other species [72]. Moreover, captivity tends to humanize the NHP microbiome, resulting in greater resemblance [2]. The main bacterial genera reported to be present in the gut microbiome of both NHPs and humans are *Faecalibacterium*, *Prevotella*, *Bacteroides*, *Streptococcus*, *Treponema*, *Megasphaera*, *Bifidobacterium*, *Alistipes*, *Collinsella*, *Escherichia* and *Ruminococcus* [2, 9]. This is in line with our data. Although there are inherent differences in microbiome profiles between humans and macaques, our study represents domain adaptation scenarios in which the source domain is derived from humans and the target domain is derived from macaques. Domain adaptation is commonly employed to align different datasets to apply models across both domains [73]. The results of our macaque test dataset indicate that this approach is applicable.

Within the constraints of the current dataset, we aimed to select functional groups to demonstrate the ability of our ML/DL model to discriminate groups. Although the *Firmicutes/Bacteroidetes* (F/B) ratio is a widely accepted marker in the human microbiome for maintaining normal intestinal homeostasis, this ratio does not reflect the same dynamics in rhesus macaques [74–76]. Human feces are dominated by *Bacteroidetes*, whereas rhesus macaque feces have a more evenly distributed relative abundance of *Firmicutes* and *Bacteroidetes* [31]. Since butyrate has known beneficial effects on colonic function in health and disease and is formed by certain members that generally form separate groups, we selected butyrate-producing groups and mixed fermenters as alternative functional groups [77–79].

Compared with control animals without diarrhea, rhesus macaques with chronic diarrhea present different gut microbiome signatures [9, 13, 14]. Consistent with our results, within the butyrate-producing group, *Coprococcus*, *Dysosmobacter*, and *Clostridium* have been reported to differ significantly between animals with and without diarrhea [9, 14]. For the mixed fermenter group, even more genera corresponded with our results: *Treponema*, *Oscillibacter*, *Pseudomonas*, *Bacillus*, *Streptomyces*, *Clostridioides* and *Bacteroides* [9]. Although other genera have also been reported, the above highlights the importance of detecting more genera or groups. These findings are valuable for diagnosing and monitoring gut health and demonstrate the clinical utility of our approach to fecal imaging.

The success in predicting both functional groups and bacterial genera likely originates from the model capturing visual features influenced by microbial metabolic activities. Microbial enterotypes are correlated with both fecal consistency and color [80, 81]. Diet and subsequent effects on the physiochemical colonic environment and metabolic byproducts can alter fecal pH and fecal consistency, affecting the texture and glossiness visible in images [82, 83]. Enhanced fermentation alters the physical structure of feces, potentially resulting in more homogeneous smears with distinct characteristics. This is supported by observations in NHPs, where stool consistency was influenced by fiber intake: low-fiber diets resulted in clay-like stools, whereas high-fiber diets produced softer and bulkier stools [84].

Understanding the internal mechanisms of AI models is essential for their acceptance in clinical settings. The decisions made by AI models should be guided by relevant biological data rather than spurious shortcuts or confounding factors. Research has shown that DL models

can sometimes rely on spurious shortcuts such as hospital-specific imaging artifacts and patient positioning rather than true pathological signals [85]. Although less frequently reported, similar pitfalls have been observed in veterinary imaging studies on canine radiographs [86]. However, in image-based AI models, deriving factors that are invariant to confounding factors can reduce these irrelevant and biased associations [87]. In our study, potential confounders such as diet-related color, smearing methods, and fecal weights were rigorously examined through preprocessing (grayscale) perturbation experiments and correlation analysis. Our model demonstrated robust confounding effects from these confounders.

Another crucial consideration of AI models is their practical applicability. Defecation output and volume vary significantly across species and individuals. If a model's predictions heavily depend on the fecal weight, this could substantially limit its practical use. Our model's prediction was not dependent on the amount of fecal matter, as no correlation was observed between the fecal weight on the smear and the prediction probability.

Furthermore, images are sensory data obtained from cameras, each with different resolutions and levels of random noise [88]. Our perturbation experiments reveal that image blurring reduces model performance, highlighting the importance of high resolution in cameras. However, the model's performance remained stable in the presence of random Gaussian noise, suggesting that while high camera resolution is crucial, random noise from the camera does not substantially impact the model. It is important to note that we have investigated the effects of Gaussian noise only, as Gaussian noise is a common occurrence in images. Other types of noise, such as structured noise or salt-and-pepper noise, were not explored in our study [88].

While our results are promising, it is important to acknowledge limitations. The sample size was relatively small, and further studies with larger macaque-specific datasets would be beneficial to validate our results and to refine our model further. It is possible that domain adaptation limits the detection of macaque-specific genera. Currently, cohorts of humans, farms and companion animals are being collected and analyzed. Future studies should include cross-species validation.

Furthermore, focusing on the extremes of our data distribution, i.e., the top and bottom 10%, enhances the statistical power but results in a lack of generalizability in the model. This binary classification threshold is inherently dataset dependent. However, this approach is common in exploratory microbiome studies to highlight biologically meaningful differences. As our dataset expands and becomes more standardized, the thresholds may be recalibrated, and the use of regression models to further refine the predictive performance can be explored.

Furthermore, this paper conceptualizes image properties into local and global features and conducts experiments on the basis of this framework. However, investigating how specific features, such as shape, color, granularity, and texture, e.g., consistency or smoothness, contribute to the model's performance in detail would be valuable.

Specific bacterial genera can contribute to specific color changes in feces [80]. Yet, due the use of colored dietary markers, our fecal images had to be converted to grayscale images, possibly resulting in underperformance of the model.

The gut microbiome comprises at least 130 bacterial genera [89]. Although many abundant genera are identified by our model, this is still a small portion of the full extent of the gut microbiome. In addition, describing clear group functionality is challenging because bacteria can be functionally convergent, and the microbiota is a highly dynamic ecosystem [83, 90].

Compositional and functional alterations in the normal gut microbiome, i.e., dysbiosis, have been associated with various diseases in humans, companion animals and large animals [79, 91–97]. The high costs and prolonged turnaround times limit the clinical application of microbiome sequencing for patients [96]. Our approach could offer a cost-effective way to assess the impact of drug or nutritional interventions on the microbiome. In companion animal research where the gut microbiota is assessed, underpowered studies due to limited funding availability are not uncommon [93]. In addition, microbiome testing is a useful tool in veterinary medicine, as many diseases in many animal species are associated with gut imbalances [91, 93, 94, 96]. Some of these imbalances can be detected via microbiome screening before a patient becomes symptomatic [93]. On the other hand, to evaluate the effectiveness of interventions, it may be feasible to screen the microbiome before and after treatment [93, 98, 99]. Furthermore, longitudinal assessments of the gut microbiome in large human cohorts within citizen science research potentially provide valuable insights through our affordable approach [100]. Currently, the dysbiosis index is an upcoming diagnostic tool for companion animals to diagnose and follow up on interventions [96, 98, 99, 101]. The dysbiosis index (DI) is based on quantitative PRC assays of bacterial groups on fecal DNA. As we are expanding our model with data from species other than macaques, we could predict DI for different animal species. Antibiotic treatments could be reduced, and patient-specific dietary interventions could be utilized more frequently, ultimately improving animal health and welfare through the introduction of this novel diagnostic tool.

Conclusions

Our method not only detects important bacterial genera but also identifies microbial groups on the basis of their assigned function in the gut microbiome. In addition, the models were robust to the smearing method, random noise, and amount of fecal matter used for the smear. These findings demonstrate the potential of this method as a clinically applicable tool for rapid microbiome diagnosis in veterinary science. Furthermore, it provides a cost-effective approach for assessing the impact of drugs or nutrition interventions on the microbiome.

Acknowledgements
The authors would like to thank the Animal Science department of the BPRC, especially the animal caretakers for excellent care of the animals and for assisting with sample collection and Nicole Heijmans for assisting with the fecal smears. Francisca van Hassel for figure design and Thea de Koning for her assistance with editing the manuscript.

Author contributions
Conceptualization: A.M., D.L., E.L. Methodology: D.L., E.L. Software: D.L., H.N., E.L. Formal analysis and validation: D.L., H.N, E.L. Investigation: A.M., D.L., J.B., E.L. Resources: A.M., D.L., R.M., J.B., J.A.M.L., E.L Data curation: A.M., D.L., E.L Writing-original draft preparation: A.M., D.L., E.L. Writing-review and editing: H.N., R.M., J.A.M.L., J.B., E.L. Supervision: R.M., J.B., J.A.M.L., E.L. All authors have read and approved the final manuscript.

Funding
No external funding was received.

Data availability
Sequence data that support the findings of this study have been deposited in the European Nucleotide Archive https://www.ebi.ac.uk/ena/browser/view/PRJEB70928.

Declarations

Ethical approval
All animals were housed in accordance with Dutch law and international ethical and scientific standards and guidelines (EU Directive 63/2010). All procedures and husbandry were compliant with the above standards and legislation. No interventions other than those required for veterinary care were performed on these animals; therefore, no approval from the competent authorities was needed. Nevertheless, additional approval was obtained from the institutional animal welfare body (IvD 018 A). The Biomedical Primate Research Centre (BPRC) is accredited by the Association for Assessment and Accreditation of Laboratory Animal Care (AAALAC) International.

Consent for publication
Not applicable.

Competing interests
E. Levin is the founder of HORAIZON BV, the Netherlands, which owns a patent related to the technology used (Patent No. WO2023055238A1). This has no relevance to the content of the current paper. The other authors declare no competing interests.

Author details
[1]Biomedical Primate Research Centre, Lange Kleiweg 161, Rijswijk 2288 GJ, Netherlands
[2]Department Population Health Sciences, Animals in Science and Society, Faculty of Veterinary Medicine, Utrecht University, Yalelaan 2, Utrecht 3584 CM, Netherlands
[3]HORAIZON Technology BV, Marshallaan 2, Delft 2625 GZ, Netherlands

Received: 18 January 2025 / Accepted: 12 April 2025
Published online: 24 April 2025

References

1. Amato KR, Song JGS, Nute SJ, Metcalf M, Thompson JL, Morton LR, Amir JT, V A, Humphrey JM. Evolutionary trends in host physiology outweigh dietary niche in structuring primate gut microbiomes. ISME J. 2019;13(3):576–87.
2. Clayton JB, Vangay P, Huang H, Ward T, Hillmann BM, Al-Ghalith GA, Travis DA, Long HT, Tuan BV, Minh VV, et al. Captivity humanizes the primate Microbiome. Proc Natl Acad Sci U S A. 2016;113(37):10376–81.
3. Amato KR, Yeoman CJ, Cerda G, Schmitt CA, Cramer JD, Miller ME, Gomez A, Turner TR, Wilson BA, Stumpf RM, et al. Variable responses of human and non-human primate gut microbiomes to a Western diet. Microbiome. 2015;3:53.
4. Lozupone CA, Stombaugh JI, Gordon JI, Jansson JK, Knight R. Diversity, stability and resilience of the human gut microbiota. Nature. 2012;489(7415):220–30.
5. Yildirim S, Yeoman CJ, Sipos M, Torralba M, Wilson BA, Goldberg TL, Stumpf RM, Leigh SR, White BA, Nelson KE. Characterization of the fecal Microbiome from non-human wild primates reveals species specific microbial communities. PLoS ONE. 2010;5(11):e13963.
6. Hamer HM, Jonkers D, Venema K, Vanhoutvin S, Troost FJ, Brummer RJ. Review Article: the role of butyrate on colonic function. Aliment Pharmacol Ther. 2008;27(2):104–19.
7. Laing ST, Merriam D, Shock BC, Mills S, Spinner A, Reader R, Hartigan-O'Connor DJ. Idiopathic colitis in Rhesus macaques is associated with dysbiosis, abundant enterochromaffin cells and altered T-Cell cytokine expression. Vet Pathol. 2018;55(5):741–52.
8. Walker AW, Sanderson JD, Churcher C, Parkes GC, Hudspith BN, Rayment N, Brostoff J, Parkhill J, Dougan G, Petrovska L. High-throughput clone library analysis of the mucosa-associated microbiota reveals dysbiosis and differences between inflamed and non-inflamed regions of the intestine in inflammatory bowel disease. BMC Microbiol. 2011;11:7.
9. Yang S, Liu Y, Yang N, Lan Y, Lan W, Feng J, Yue B, He M, Zhang L, Zhang A, et al. The gut Microbiome and antibiotic resistome of chronic diarrhea rhesus macaques (Macaca mulatta) and its similarity to the human gut Microbiome. Microbiome. 2022;10(1):29.
10. Ardeshir A, Oslund KL, Ventimiglia F, Yee J, Lerche NW, Hyde DM. Idiopathic microscopic colitis of rhesus macaques: quantitative assessment of colonic mucosa. Anat Rec (Hoboken). 2013;296(8):1169–79.
11. Prongay K, Park B, Murphy SJ. Risk factor analysis May provide clues to diarrhea prevention in outdoor-housed rhesus macaques (Macaca mulatta). Am J Primatol. 2013;75(8):872–82.
12. Sestak K, Merritt CK, Borda J, Saylor E, Schwamberger SR, Cogswell F, Didier ES, Didier PJ, Plauche G, Bohm RP, et al. Infectious agent and immune response characteristics of chronic Enterocolitis in captive rhesus macaques. Infect Immun. 2003;71(7):4079–86.
13. Maaskant A, Voermans B, Levin E, de Goffau MC, Plomp N, Schuren F, Remarque EJ, Smits A, Langermans JAM, Bakker J, et al. Microbiome signature suggestive of lactose-intolerance in rhesus macaques (Macaca mulatta) with intermittent chronic diarrhea. Anim Microbiome. 2024;6(1):53.
14. Compo NR, Mieles-Rodriguez L, Gomez DE. Fecal bacterial microbiota of healthy Free-Ranging, healthy corralled, and chronic diarrheic corralled Rhesus macaques (Macaca mulatta). Comp Med. 2021;71(2):152–65.
15. McGrew K, de Oca NM, Kosten TA. Effect of relocation, social housing changes, and diarrhea status on Microbiome composition of juvenile Cynomolgus macaques (Macaca fascicularis). Microorganisms. 2025;13:98.
16. Westreich ST, Ardeshir A, Alkan Z, Kable ME, Korf I, Lemay DG. Fecal metatranscriptomics of macaques with idiopathic chronic diarrhea reveals altered mucin degradation and fucose utilization. Microbiome. 2019;7(1):41.
17. Knight R, Vrbanac A, Taylor BC, Aksenov A, Callewaert C, Debelius J, Gonzalez A, Kosciolek T, McCall LI, McDonald D et al. Best practices for analysing microbiomes. In: Nature Reviews Microbiology. Nature Publishing Group. 2018;16:410–422.
18. Biddle A, Stewart L, Blanchard J, Leschine S. Untangling the genetic basis of fibrolytic specialization by lachnospiraceae and ruminococcaceae in diverse gut communities. Diversity. 2013;5(3):627–40.
19. Flint HJ, Scott KP, Duncan SH, Louis P, Forano E. Microbial degradation of complex carbohydrates in the gut. Gut Microbes. 2012;3(4):289–306.
20. Fonseca DC, da Rocha Fernandes G, Waitzberg DL. Artificial intelligence and human microbiome: A brief narrative review. Clin Nutr Open Sci. 2025;59:134–42.
21. Abavisani M, Khoshrou A, Foroushan SK, Ebadpour N, Sahebkar A. Deciphering the gut microbiome: the revolution of artificial intelligence in microbiota analysis and intervention. Curr Res Biotechnol. 2024;7:100211.

22. Hernández Medina R, Kutuzova S, Nielsen KN, Johansen J, Hansen LH, Nielsen M, Rasmussen S. Machine learning and deep learning applications in Microbiome research. ISME Commun 2022, 2(1).
23. Craddock HA, Godneva A, Rothschild D, Motro Y, Grinstein D, Lotem-Michaeli Y, Narkiss T, Segal E, Moran-Gilad J. Phenotypic correlates of the working dog Microbiome. NPJ Biofilms Microbiomes. 2022;8(1):66.
24. Monteiro HF, Figueiredo CC, Mion B, Santos JEP, Bisinotto RS, Penagaricano F, Ribeiro ES, Marinho MN, Zimpel R, da Silva AC, et al. An artificial intelligence approach of feature engineering and ensemble methods depicts the rumen Microbiome contribution to feed efficiency in dairy cows. Anim Microbiome. 2024;6(1):5.
25. Zhang B, Lin S, Moraes L, Firkins J, Hristov AN, Kebreab E, Janssen PH, Bannink A, Bayat AR, Crompton LA, et al. Methane prediction equations including genera of rumen bacteria as predictor variables improve prediction accuracy. Sci Rep. 2023;13(1):21305.
26. Ballard ZS, Brown C, Ozcan A. Mobile technologies for the discovery, analysis, and engineering of the global Microbiome. ACS Nano. 2018;12(4):3065–82.
27. Furusawa C, Tanabe K, Ishii C, Kagata N, Tomita M, Fukuda S. Decoding gut microbiota by imaging analysis of fecal samples. iScience. 2021;24(12):103481.
28. Lee D, Maaskant A, Ngo H, Montijn RC, Bakker J, Langermans JAM, Levin E. A rapid, affordable, and reliable method for profiling Microbiome biomarkers from fecal images. iScience. 2024;27(12):111310.
29. van de Put M, van den Belt M, de Wit N, Kort R. Rationale and design of a randomized placebo-controlled nutritional trial embracing a citizen science approach. Nutr Res. 2024;131:96–110.
30. Amann J, Blasimme A, Vayena E, Frey D, Madai VI. Precise Qc: explainability for artificial intelligence in healthcare: a multidisciplinary perspective. BMC Med Inf Decis Mak. 2020;20(1):310.
31. Chen S, Zhou Y, Chen Y, Gu J. Fastp: an ultra-fast all-in-one FASTQ preprocessor. Bioinformatics. 2018;34(17):i884–90.
32. Wood DE, Lu J, Langmead B. Improved metagenomic analysis with kraken 2. Genome Biol. 2019;20(1):257.
33. Sayers EW, Bolton EE, Brister JR, Canese K, Chan J, Comeau DC, Connor R, Funk K, Kelly C, Kim S, et al. Database resources of the National center for biotechnology information. Nucleic Acids Res. 2022;50(D1):D20–6.
34. Lu J, Breitwieser FP, Thielen P, Salzberg SL. Bracken: estimating species abundance in metagenomics data. PeerJ Comput Sci. 2017;3:e104.
35. Gruning B, Dale R, Sjodin A, Chapman BA, Rowe J, Tomkins-Tinch CH, Valieris R, Koster J, Bioconda T. Bioconda: sustainable and comprehensive software distribution for the life sciences. Nat Methods. 2018;15(7):475–6.
36. Lee D, Maaskant A, Ngo H, Montijn RC, Bakker J, Langermans JAM, Levin E. A rapid, affordable, and reliable method for profiling Microbiome biomarkers from fecal images. iScience 2024, 27(12).
37. Dosovitskiy A, Beyer L, Kolesnikov A, Weissenborn D, Zhai X, Unterthiner T, Dehghani M, Minderer M, Heigold G, Gelly S et al. An Image is Worth 16x16 Words: Transformers for Image Recognition at Scale. International Conference on Learning Representations (ICLR) arXiv:201011929 2021.
38. Steiner A, XKolesnikov A, Zhai X, Wightman R, Uszkoreit J, Beyer L. How to train your ViT? Data, Augmentation, and Regularization in Vision Transformers. arXiv:210610270 2021.
39. Radford A, Wook Kim J, Hallacy C, Ramesh A, Goh G, Agarwal S, Sastry G, Askell A, Mishkin P, Clark J, et al. Learning transferable visual models from natural Language supervision. Int Conf Mach Learn (ICML). 2021. arXiv:210300020.
40. Caron M, Touvron H, Misra I, Jégou H, Mairal J, Bojanowski P, Joulin A. Emerging properties in Self-Supervised vision Transformers. Int Conf Comput Vis (ICCV). 2021. arXiv:210414294.
41. He K, Zhang X, Ren S, Sun J. Identity Mappings in Deep Residual Networks. European Conference on Computer Vision (ECCV) arXiv:160305027 2016.
42. Kolesnikov A, Beyer L, Zhai X, Puigcerver J, Yung J, Gelly S, Houlsby N. Big Transfer (BiT): General Visual Representation Learning. *European Conference on Computer Vision (ECCV) arXiv:191211370* 2019.
43. Tibshirani R. Regression shrinkage and selection via the Lasso. J Royal Stat Soc Ser B (Methodological). 1996;58(1):267–88.
44. Hanley JA, McNeil BJ. The meaning and use of the area under a receiver operating characteristic (ROC) curve. Radiology. 1982;143(1):29–36.
45. Paszke A, Gross S, Massa F, Lerer A, Bradbury J, Chanan G, Killeen T, Lin Z, Gimelshein N, Antiga L. Pytorch: an imperative style, high-performance deep learning library. Adv Neural Inf Process Syst 2019, 32.
46. Pedregosa F, Varoquaux G, Gramfort A, Michel V, Thirion B, Grisel O, Blondel M, Weiss R, Dubourg V, Vanderplas J, et al. Scikit-learn: machine learning in Python Gaël Varoquaux Bertrand thirion Vincent Dubourg Alexandre Passos PEDREGOSA, VAROQUAUX, GRAMFORT ET AL. Matthieu Perrot. J Mach Learn Res. 2011;12(85):2825–30.
47. Angelakis E, Yasir M, Bachar D, Azhar EI, Lagier JC, Bibi F, Jiman-Fatani AA, Alawi M, Bakarman MA, Robert C et al. Gut Microbiome and dietary patterns in different Saudi populations and monkeys. Sci Rep 2016, 6.
48. Bui TPN, Shetty SA, Lagkouvardos I, Ritari J, Chamlagain B, Douillard FP, Paulin L, Piironen V, Clavel T, Plugge CM, et al. Comparative genomics and physiology of the butyrate-producing bacterium intestinimonas butyriciproducens. Environ Microbiol Rep. 2016;8(6):1024–37.
49. Carlier JP, Bedora-Faure M, K'Ouas G, Alauzet C, Mory F et al. Proposal to unify Clostridium orbiscindens Winter 1991 and Eubacterium plautii (Séguin. 1928) Hofstad and Aasjord 1982, with description of Flavonifractor plautii gen. nov., comb. nov., and reassignment of Bacteroides capillosus to Pseudoflavonifractor capillosus gen. nov., comb. nov. In: International Journal of Systematic and Evolutionary Microbiology. 2010;60:585–590.
50. Detman A, Mielecki D, Chojnacka A, Salamon A, Błaszczyk MK, Sikora A. Cell factories converting lactate and acetate to butyrate: Clostridium butyricum and microbial communities from dark fermentation bioreactors. Microb Cell Fact 2019, 18(1).
51. Frimmersdorf E, Horatzek S, Pelnikevich A, Wiehlmann L, Schomburg D. How Pseudomonas aeruginosa adapts to various environments: A metabolomic approach. Environ Microbiol. 2010;12(6):1734–47.
52. Hesketh AR, Chandra G, Shaw AD, Rowland JJ, Kell DB, Bibb MJ, Chater KF. Primary and secondary metabolism, and post-translational protein modifications, as portrayed by proteomic analysis of Streptomyces coelicolor. Mol Microbiol. 2002;46(4):917–32.
53. Iino T, Mori K, Tanaka K, Suzuki KI, Harayama S. Oscillibacter valericigenes gen. Nov., Sp. Nov., a valerate-producing anaerobic bacterium isolated from the alimentary Canal of a Japanese corbicula clam. Int J Syst Evol MicroBiol. 2007;57(8):1840–5.
54. Ikeyama N, Murakami T, Toyoda A, Mori H, Iino T, Ohkuma M, Sakamoto M. Microbial interaction between the succinate-utilizing bacterium Phascolarctobacterium faecium and the gut commensal Bacteroides thetaiotaomicron. MicrobiologyOpen 2020, 9(10).
55. Kageyama A, Benno Y. A Gram-positive anaerobic bacterium isolated from human faeces. Int J Syst Evolutionary Microbiol Vol. 2000;50:1595–9.
56. Kläring K, Hanske L, Bui N, Charrier C, Blaut M, Haller D, Plugge CM, Clavel T. Intestinimonas butyriciproducens gen. Nov., Sp. Nov., a butyrate-producing bacterium from the mouse intestine. Int J Syst Evol MicroBiol. 2013;63(PART 12):4606–12.
57. Le Roy T, Moens De Hase E, Van Hul M, Paquot A, Pelicaen R, Régnier M, Depommier C, Druart C, Everard A, Maiter D, et al. Dysosmobacter welbionis is a newly isolated human commensal bacterium preventing diet-induced obesity and metabolic disorders in mice. Gut. 2022;71(3):534–43.
58. Lin X, Hu T, Wu Z, Li L, Wang Y, Wen D, Liu X, Li W, Liang H, Jin X et al. Isolation of potentially novel species expands the genomic and functional diversity of Lachnospiraceae. iMeta 2024, 3(2).
59. Louis P, Flint HJ. Diversity, metabolism and microbial ecology of butyrate-producing bacteria from the human large intestine. FEMS Microbiol Lett. 2009;294(1):1–8.
60. Makovska M, Killer J, Modrackova N, Ingribelli E, Amin A, Vlkova E, Bolechova P, Neuzil-Bunesova V. Species and strain variability among Sarcina isolates from diverse mammalian hosts. Animals 2023, 13(9).
61. Salazar-Jaramillo L, de la Cuesta-Zuluaga J, Chica LA, Cadavid M, Ley RE, Reyes A, Escobar JS. Gut Microbiome diversity within Clostridia is negatively associated with human obesity. mSystems 2024, 9(8).
62. Seo B, Jeon K, Baek I, Lee YM, Baek K, Ko GP. Faecalibacillus intestinalis gen. Nov., Sp. Nov. And Faecalibacillus faecis Sp. Nov., isolated from human faeces. Int J Syst Evol MicroBiol. 2019;69(7):2120–8.
63. Shin JH, Tillotson G, MacKenzie TN, Warren CA, Wexler HM, Goldstein EJC. Bacteroides and related species: The keystone taxa of the human gut microbiota. In: Anaerobe. Academic Press 2024; 85.
64. Shkoporov AN, Chaplin AV, Kafarskaia LI, Efimov BA. Ruthenibacterium. Bergey's Manual of Systematics of Archaea and Bacteria. Wiley; 2019;1–8.
65. Singh V, Lee GD, Son HW, Koh H, Kim ES, Unno T, Shin JH. Butyrate producers, The Sentinel of Gut: Their intestinal significance with and beyond butyrate, and prospective use as microbial therapeutics. In: Frontiers in Microbiology. Frontiers Media S.A. 2023; 13.
66. Song CH, Kim N, Nam RH, Choi SI, Jang JY, Lee HN. Changes in gut Microbiome upon orchiectomy and testosterone administration in AOM/DSS-Induced Colon cancer mouse model. Cancer Res Treat. 2023;55(1):196–218.

67. Tan X, Wu J, Zhang H, Li Y, Huang Y, Zheng P, Xie P. Biogeography of intestinal mucus-associated microbiome: depletion of genus Pseudomonas is associated with depressive-like behaviors in female cynomolgus macaques. J Adv Res 2024.
68. Wang J, Shen C, Sun J, Cheng L, Zhao G, Li MM. Metagenomic analysis reveals a dynamic rumen Microbiome with diversified adaptive functions in response to dietary protein restriction and re-alimentation. Sci Total Environ 2024, 949.
69. Zafar H, Saier MH. Gut Bacteroides species in health and disease. Gut microbes. Volume 13. Bellwether Publishing, Ltd.; 2021. pp. 1–20.
70. Machiels K, Joossens M, Sabino J, De Preter V, Arijs I, Eeckhaut V, Ballet V, Claes K, Van Immerseel F, Verbeke K, et al. A decrease of the butyrate-producing species Roseburia hominis and Faecalibacterium prausnitzii defines dysbiosis in patients with ulcerative colitis. Gut. 2014;63(8):1275–83.
71. Scheithauer TPM, Montijn RC, Mieremet A. Gut microbe-host interactions in post-COVID syndrome: a debilitating or restorative partnership? Gut Microbes. 2024;16(1):2402544.
72. Nagpal R, Wang S, Solberg Woods LC, Seshie O, Chung ST, Shively CA, Register TC, Craft S, McClain DA, Yadav H. Comparative Microbiome signatures and Short-Chain fatty acids in mouse, rat, Non-human primate, and human feces. Front Microbiol. 2018;9:2897.
73. Orouji S, Liu MC, Korem T, Peters MAK. Domain adaptation in small-scale and heterogeneous biological datasets. Sci Adv. 2024;10(51):eadp6040.
74. Ley RE, Turnbaugh PJ, Klein S, Gordon JI. Microbial ecology: human gut microbes associated with obesity. Nature. 2006;444(7122):1022–3.
75. Li W, Ma ZS. FBA ecological guild: trio of Firmicutes-Bacteroidetes alliance against Actinobacteria in human oral Microbiome. Sci Rep. 2020;10(1):287.
76. Petakh P, Oksenych V, Kamyshnyi A. The F/B ratio as a biomarker for inflammation in COVID-19 and T2D: impact of Metformin. Biomed Pharmacother. 2023;163:114892.
77. Kircher B, Sabrina W, Frank G, Dirk S, Robert G, Heike B, Vital M. Predicting butyrate- and propionate-forming bacteria of gut microbiota from sequencing data. Gut Microbes. 2022;14(1):2149019.
78. Louis P, Flint HJ. Formation of propionate and butyrate by the human colonic microbiota. Environ Microbiol. 2017;19(1):29–41.
79. Van-Wehle T, Vital M. Investigating the response of the butyrate production potential to major fibers in dietary intervention studies. Npj Biofilms Microbiomes. 2024;10(1):63.
80. Castano-Rodriguez N, Underwood AP, Merif J, Riordan SM, Rawlinson WD, Mitchell HM, Kaakoush NO. Gut Microbiome analysis identifies potential etiological factors in acute gastroenteritis. Infect Immun 2018, 86(7).
81. Vandeputte D, Falony G, Vieira-Silva S, Tito RY, Joossens M, Raes J. Stool consistency is strongly associated with gut microbiota richness and composition, enterotypes and bacterial growth rates. Gut. 2016;65(1):57–62.
82. Lewis SJ, Heaton KW. Increasing butyrate concentration in the distal colon by accelerating intestinal transit. Gut. 1997;41(2):245–51.
83. Saito Y, Sagae T. Defecation status, intestinal microbiota, and habitual diet are associated with the fecal bile acid composition: a cross-sectional study in community-dwelling young participants. Eur J Nutr. 2023;62(5):2015–26.
84. Brodribb AJ, Condon RE, Cowles V, DeCosse JJ. Effect of dietary fiber on intraluminal pressure and myoelectrical activity of left colon in monkeys. Gastroenterology. 1979;77(1):70–4.
85. DeGrave AJ, Janizek JD, Lee S-I. AI for radiographic COVID-19 detection selects shortcuts over signal. Nat Mach Intell. 2021;3(7):610–9.
86. Burti S, Zotti A, Banzato T. Role of AI in diagnostic imaging error reduction. Front Vet Sci. 2024;11:1437284.
87. Zhao Q, Adeli E, Pohl KM. Training confounder-free deep learning models for medical applications. Nat Commun. 2020;11(1):6010.
88. Boyat AK, Joshi BK. A review paper: noise models in digital image processing (SIPIJ). Signal Image Processing: Int J. 2015;6(2):63–75.
89. Rosenberg E. Diversity of bacteria within the human gut and its contribution to the functional unity of holobionts. NPJ Biofilms Microbiomes. 2024;10(1):134.
90. La Reau AJ, Suen G. The Ruminococci: key symbionts of the gut ecosystem. J Microbiol. 2018;56(3):199–208.
91. Chaucheyras-Durand F, Sacy A, Karges K, Apper E. Gastro-Intestinal microbiota in equines and its role in health and disease: the black box opens. Microorganisms 2022, 10(12).
92. Hamer HM, Jonkers D, Venema K, Vanhoutvin S, Troost FJ, Brummer RJ. Review article: The role of butyrate on colonic function. In: *Alimentary Pharmacology and Therapeutics*. vol. 27; 2008: 104–119.
93. Jarett JK, Kingsbury DD, Dahlhausen KE, Ganz HH. Best practices for Microbiome study design in companion animal research. Front Vet Sci. 2021;8:644836.
94. Kauter A, Epping L, Semmler T, Antao EM, Kannapin D, Stoeckle SD, Gehlen H, Lubke-Becker A, Gunther S, Wieler LH, et al. The gut Microbiome of horses: current research on equine enteral microbiota and future perspectives. Anim Microbiome. 2019;1(1):14.
95. Lozupone CA, Stombaugh JI, Gordon JI, Jansson JK, Knight R. Diversity, stability and resilience of the human gut microbiota. Nat Vol. 2012;489:220–30.
96. Sung CH, Marsilio S, Chow B, Zornow KA, Slovak JE, Pilla R, Lidbury JA, Steiner JM, Park SY, Hong MP, et al. Dysbiosis index to evaluate the fecal microbiota in healthy cats and cats with chronic enteropathies. J Feline Med Surg. 2022;24(6):e1–12.
97. Walker AW, Sanderson JD, Churcher C, Parkes GC, Hudspith BN, Rayment N, Brostoff J, Parkhill J, Dougan G, Petrovska L. High-throughput clone library analysis of the mucosa-associated microbiota reveals dysbiosis and differences between inflamed and non-inflamed regions of the intestine in inflammatory bowel disease. BMC Microbiol 2011, 11.
98. Toresson L, Spillmann T, Pilla R, Ludvigsson U, Hellgren J, Olmedal G, Suchodolski JS. Clinical effects of faecal microbiota transplantation as adjunctive therapy in dogs with chronic Enteropathies-A retrospective case series of 41 dogs. Vet Sci 2023, 10(4).
99. Vecchiato CG, Sabetti MC, Sung CH, Sportelli F, Delsante C, Pinna C, Alonzo M, Erba D, Suchodolski JS, Pilla R, et al. Effect of faecal microbial transplantation on clinical outcome, faecal microbiota and metabolome in dogs with chronic enteropathy refractory to diet. Sci Rep. 2025;15(1):11957.
100. van de Put M, van den Belt M, de Wit N, Kort R. Rationale and design of a randomized placebo-controlled nutritional trial embracing a citizen science approach. Nutr Res 2024.
101. AlShawaqfeh MK, Wajid B, Minamoto Y, Markel M, Lidbury JA, Steiner JM, Serpedin E, Suchodolski JS. A dysbiosis index to assess microbial changes in fecal samples of dogs with chronic inflammatory enteropathy. FEMS Microbiol Ecol 2017, 93(11).

Publisher's note